International Compressor Engineering Conference

School of Mechanical Engineering

2022

Experimental Investigation of a Screw Spindle Vacuum Pump at Sub-Atmospheric Discharge Pressures

Thomas Werner Moesch

Paul Gustav Lemke

Konrad Klotsche

Ullrich Hesse

Follow this and additional works at: https://docs.lib.purdue.edu/icec

Experimental Investigation of a Screw Spindle Vacuum Pump at Sub-Atmospheric Discharge Pressures

Thomas Werner MOESCH*, Paul Gustav LEMKE, Konrad KLOTSCHE, Ullrich HESSE

Technische Universität Dresden, Insitute of Power Engineering, Bitzer-Chair of Refrigeration,
Cryogenics and Compressor Technology
Dresden, Germany
thomas.moesch@tu-dresden.de

* Corresponding Author

ABSTRACT

Recent studies indicate that dry-running cycloid-type screw compressors with variable rotor pitch may be very suitable for R718 (water) chillers and heat pumps. However, these studies are based on thermodynamic models rather than experimental data and there is currently no R718 screw compressor with variable rotor pitch available commercially. In this study, the performance of a screw spindle vacuum pump with variable rotor pitch is experimentally investigated for various inlet and outlet pressures below atmospheric pressure using air as a working fluid. The measured pressure range corresponds to saturated gas temperatures of R718 between 0 °C and 100 °C. The resulting performance map for air is used to estimate the potential performance with R718, using appropriate correction factors. The results are evaluated in regards to the potential of spindle screw compressors for future R718 chiller and heat pump applications.

1. INTRODUCTION

The refrigerant R718 is an important alternative to F-Gases which are regulated by e.g. EU 517/2014. Current R718 refrigeration machines mainly apply turbo compressors and are used in chiller applications (Hanslik *et al*., 2019). Chamoun *et al*. (2014) tested modified screw compressors in a R718 heat pump set up and realized COP between 4.5 and 5.5 for temperature lifts of $\Delta T = 40 \ldots 50$ K. A previous analytical study shows that cycloid-type screw vacuum pumps may also be a promising alternative for high temperature lift R718 cycles (Moesch *et al*., 2019).

An evaluation of the applicability of cycloid-type screw vacuum pumps as refrigerant compressors requires standardized performance test data. However, current standards for vacuum pump performance tests (DIN, 1983) differ from the standard of refrigeration compressors (DIN, 2017). For vacuum pump performance tests the reference discharge pressure is always 1000 hPa and the suction pressure is varied. The performance map is typically represented by a volume flow to suction pressure diagram which indicates the lowest achievable suction pressure or system pressure respectively. The limit is defined by the surge line of the compressor where the internal leakages match the displacement of the compressor and the resulting delivered volume flow is reduced to 0. The standard of refrigeration compressors requires a full performance map for different saturated suction and discharge temperatures including performance parameters like volumetric and isentropic efficiencies.

The cycloid-type vacuum compressor in this paper was not designed to be operated with pure water vapor. Therefore, it is experimentally investigated using air and a test setup based on vacuum compressor tests. The experimental data is used to derive the required performance parameters and derive an appropriate semi-empirical correlation with loss coefficients. The performance data is used to predict the compressor performance with R718 for an exemplary heat pump application.

2. EXPERIMENTAL DESIGN AND TEST PROCEDURE

2.1 Test setup
The experimental test setup is shown in Figure 1. The test setup consists of an open gas loop and a cooling water loop that is connected to an external chiller. The main components are a buffer tank, the test compressor including a muffler, a secondary vacuum pump, and two control valves. The buffer tank is used to reduce the pressure pulsation on the suction side. The secondary vacuum pump with a displacement of 96 m³/h is used to reduce the discharge pressure of the test compressor below ambient pressure and the control valves are used to set the suction and discharge pressures. The test compressor is a SIHI^{Dry} V250 spindle screw vacuum pump with a permanent magnet synchronous motor for each rotor. The motors and the inverter are water-cooled. The rotor housing is filled with glycol and contains a finned tube heat exchanger with cooling water. The motors and bearings are included in the same part of the housing.
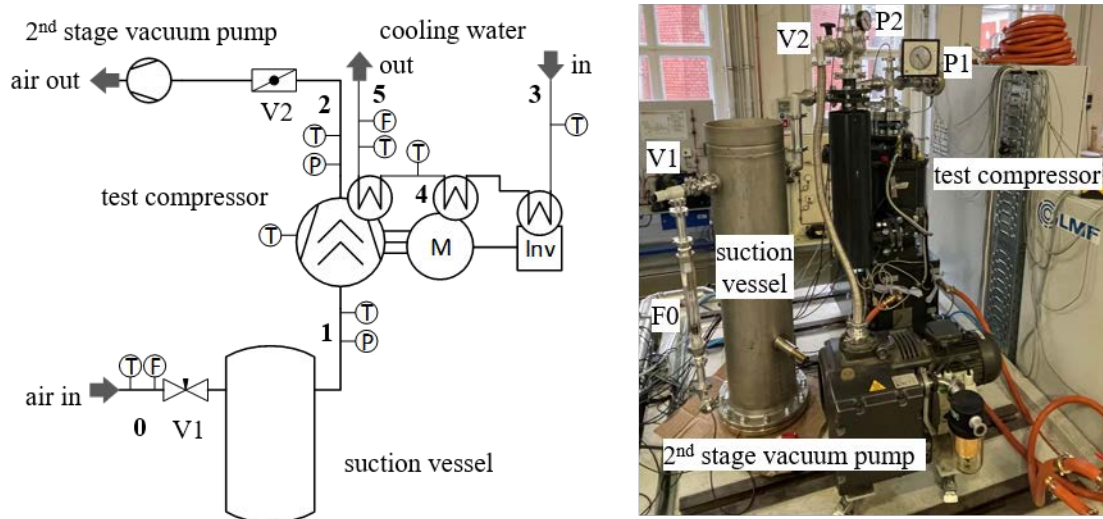
Figure 1: Test setup for sub-atmospheric compressor tests

As shown in Figure 1 the test setup is equipped with different temperature, pressure, flow, and power sensors that allow a characterization of the inlet and outlet conditions of the compressor and the compressor's overall energy balance. All sensors and their uncertainties are listed in Table 1. The suction pressure is controlled by a manual needle valve (V1) and the discharge pressure is adapted using a manual butterfly valve (V2).

Table 1: Sensors and given uncertainty

Sensor	Type	Range	Uncertainty
F0	float-type flow meter	0.5…6.5 m³/h	$\pm(0.06 \text{ m³/h} + 0.03 \times \dot{V})$
F5	velocity water meter	0.25 … 3.125 m³/h	$\pm 0.03 \times \dot{V}$ for $\dot{V} \geq 0.4$ m³/h $\pm 0.05 \times \dot{V}$ for $\dot{V} < 0.4$ m³/h
P0	aneroid barometer	960 … 1060 hPa	± 5 hPa
P1	mechanical diaphragm vacuum gauge	1 … 1000 hPa (abs.)	± 1.0 hPa for $P \leq 10$ hPa $\pm 0.1 \times P$ for $P > 10$ hPa
P2	bourdon-tube manometer	10…1020 hPa (abs.)	± 10 hPa
EP	digital power meter	0 … 6000 W	$\pm(60 \text{ W} + 0.01 \times P_{el})$
T0 … T6	PT100 (class A)	-40 °C …+180 °C	$\pm(0.15 \text{ K} + 0.002 \times |T - 273.15 \text{ K}|)$

2.2 Test matrix and control parameters

The main control parameters and their values are listed in Table 2. During the performance tests, the suction pressure p_1 and the discharge pressure p_2 were actively varied, the compressor speed was constant and the chilled water temperature and volume flow varied slightly due to the controls of the chilled water cycle. The pressures p_1 and p_2 were selected in regards to the saturated pressures of a potential R718 chiller and/or heat pump with evaporation temperatures of $\vartheta_0 = 0 \ldots 20\ °C$ and condensing temperatures of $\vartheta_C = 30 \ldots 100\ °C$.

Table 2: Control parameters and boundary condition

Parameter	Values
Suction pressure p_1 in hPa	5; 7; 9; 13; 23
Discharge pressure p_2 in hPa	40 … 1000
Ambient pressure p_0 in hPa	$1018.8 \pm 8.6^{*)}$
Ambient temperature T_0 in °C	$20.7 \pm 0.6^{*)}$
Cooling water temperature T_3 in °C	$12.2 \pm 0.1^{*)}$
Cooling water volume flow $\dot{V}_5$ in m³/h	$0.199 \pm 0.003^{*)}$
Compressor rotor speed n in min^{-1}	12,000

$^{*)}$ variance of all measured data

3. PERFORMANCE ANALYSIS

The compressor's main performance parameters are its suction volume flow $\dot{V}_{suc}$, its power consumption P_{el}, and the resulting volumetric and overall isentropic efficiency η_v and η_s. The suction volume flow $\dot{V}_{suc}$ is derived from the measured flow $\dot{V}_0$ at ambient conditions assuming a mass balance in the buffer tank.

$$\dot{V}_{suc} = \dot{V}_1 = (\rho_0/\rho_1) \cdot \dot{V}_0 \tag{1}$$

The volumetric efficiency is based on the geometrically defined displacement volume V_{disp} and the compressor rotor speed n. According to Moesch *et al.* (2019), the displacement volume V_{disp} of the tested compressor is 434.5 cm³.

$$\eta_v = \rho_0 \dot{V}_0 / (\rho_1 n V_{disp}) \tag{2}$$

The overall isentropic efficiency $\eta_{s,tot}$ is the ratio of the isentropic power input P_s and the power consumption P_{el} and it includes the indicated isentropic efficiency $\eta_{s,i}$, a mechanical efficiency η_m, and an electrical efficiency η_{el}.

$$\eta_{s,tot} = P_s/P_{el} = \eta_{s,i} \cdot \eta_m \eta_{el} \tag{3}$$

$$\text{with} \quad P_s = \rho_0 \dot{V}_0 \cdot (h_{2,s} - h_1)$$

The combined mechanical and electrical efficiency $\eta_m \eta_{el}$ is the ratio of the power input P_i (indicated power) that is ultimately transferred to the gas during compression and the power consumption P_{el}. It is derived from the heat output $\dot{Q}_{3-4}$ of the inverter, the motor, and the bearings.

$$\eta_m \eta_{el} = P_i/P_{el} = 1 - \dot{Q}_{3-4}/P_{el} \tag{4}$$

$$\text{with} \quad \dot{Q}_{3-4} = c_{p,w} \rho_w \dot{V}_w \cdot (T_4 - T_3)$$

The indicated isentropic efficiency $\eta_{s,i}$ is the ratio of the isentropic power input P_s and the indicated power P_i.

$$\eta_{s,i} = P_s/P_i = P_s/\left(P_{el} - \dot{Q}_{3-4}\right) \tag{5}$$

A further loss coefficient analysis requires theoretical values for the inner efficiency and the indicated power input. Eq. (6) defines the theoretical indicated isentropic efficiency $\eta_{s,i,th}$ as the ratio of the specific isentropic work w_s and the indicated work w_i that includes over- and under-compression losses in regards to the volume index V_i. The geometry calculations of Moesch *et al.* (2019) show that the volume index V_i of this test compressor is 6.8. In contrast to $\eta_{s,i}$, $\eta_{s,i,th}$ assumes a compression without internal leakages ($m = const.$).

$$\eta_{s,i,th} = w_s/w_i = \left(h_{2,s} - h_1\right)/\left[h_{2,s,i} - h_1 + \left(p_2 - p_{2,i}\right)\cdot v_{2,i}\right] \tag{6}$$
$$\text{with} \quad v_{2,i} = v_1 \cdot V_i \quad \text{and} \quad h_{2,s,i} = h\left(p_{2,i}, s_1\right) \quad \text{and} \quad p_{2,i} = p\left(v_{2,i}, s_1\right) \quad \text{and} \quad h_{2,s} = h\left(p_2, s_1\right)$$

The theoretical indicated power input $P_{i,th}$ is based on the assumption of an ideal machine ($\eta_v = 1$) and it is defined by Eq. (7). In further contrast to the measured P_i as defined in Eq. (5), $P_{i,th}$ does not include internal leakage losses.

$$P_{i,th} = V_{disp} \cdot n \cdot w_i = V_{disp} \cdot n \cdot \left[h_{2,s,i} - h_1 + \left(p_2 - p_{2,i}\right)\cdot v_{2,i}\right] \tag{7}$$

All fluid properties such as v, ρ, s, h, and c_p were calculated using CoolProp (Bell *et al.*, 2014). The error propagation is evaluated based on the Taylor Series Method described by Coleman and Steele (2009) and the uncertainties of the fluid properties are approximated by a central-difference approach.

4. EXPERIMENTAL RESULTS AND LOSS COEFFICIENTS

4.1 Volumetric efficiency and flow regime
Figure 2 shows the volumetric efficiency over the pressure ratio p_2/p_1 for the different suction pressures p_1. For the tested suction pressures, the volumetric efficiency is between 0.65 and 0.85. For each suction pressure, the volumetric efficiency changes only slightly (± 0.05) in regard to the vast range of pressure ratios ($p_2/p_1 = 4.3\ldots 200$). The volumetric efficiency increases with decreasing suction pressures. This phenomenon may be contributed to the rarefied gas flow regime of the leakage flows. For the tested suction pressure range and the possible minimal leakage gap heights of $h_{min}= 0.05\ldots 0.30$ mm, the Knudsen number (see Eq.(8)) is within $0.01 \leq Kn \leq 0.1$. This indicates a slip flow regime according to Huck *et al.* (2018). Within this regime, the relative leakage flow increases with higher inlet pressure or lower Kn respectively. Thus the volumetric efficiency decreases with higher inlet pressures.
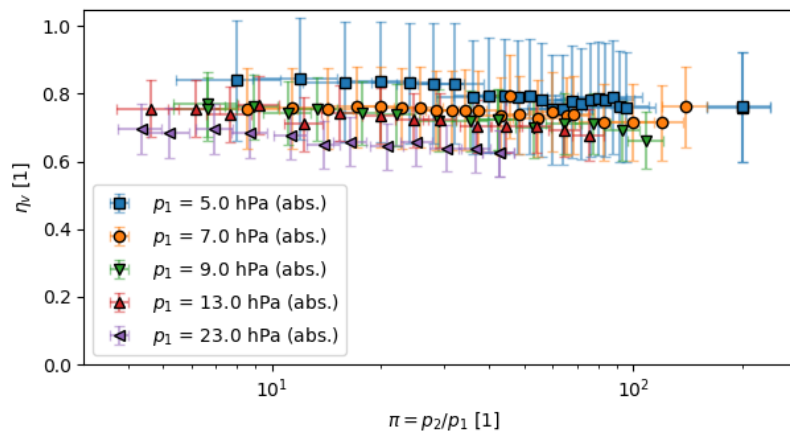
**Figure 2:** Measured volumetric efficiency for various suction pressures and pressure ratios

$$Kn = \frac{\mu \cdot c_m \cdot \sqrt{\pi}}{2 \cdot h_{min} \cdot p} \tag{8}$$

$$\text{with} \quad c_m = (2 \cdot k \cdot T)^{0.5}(M/N)^{-0.5}$$

Where $k = 1.380649 \times 10^{-23}$ J/K is the Boltzmann constant and $N = 6.02214086 \times 10^{23}$ mol^{-1} is the Avogadro constant, M is the molar mass and μ is the dynamic viscosity.

4.2 Isentropic, inner, mechanical, and electrical efficiency

Figure 3 shows η_s over the pressure ratio $\pi = p_2/p_1$ for the different suction pressures p_1. The results show a characteristic efficiency curve for positive displacement compressors with internal compression for each p_1. Each efficiency curve has an optimum pressure ratio π_{opt}, steeply decreases for $\pi \rightarrow 1$ and steadily decreases for $\pi \rightarrow \infty$. The optimum pressure ratio shifts towards lower values for increasing suction pressures. The overall isentropic effiency of the tested compressor reaches a maximum value of 0.325 within the measured suction pressure range. This is rather low compared to state-of-the-art refrigeration piston compressors which reach $\eta_{s,tot}$ values between 0.6 and 0.7 (Edler, 2014).
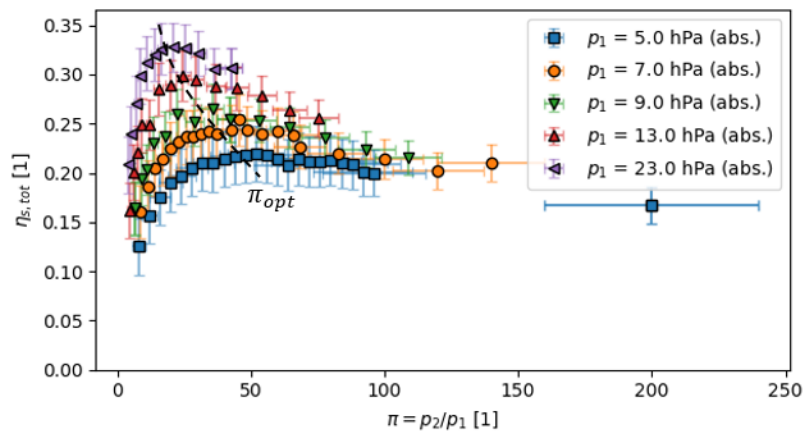
Figure 3: Measured overall isentropic efficiency $\eta_{s,tot}$ for various suction pressures and pressure ratios

Figure 4 shows the measured η_i, which represents the performance of the actual rotor profile. The trend $\eta_{s,i}$ follows the theoretical $\eta_{s,i,th}$ but has an offset that decreases with increasing pressure ratios. This offset represents all inner losses at the rotor but mainly inner leakage losses. The decrease in leakage losses may be linked to decreased leakage gap sizes due to increased thermal deformation of the rotors at higher pressure ratios. In regard to the wide range of pressure ratios the efficiency values are acceptable even compared to state-of-the-art refrigerant compressors.
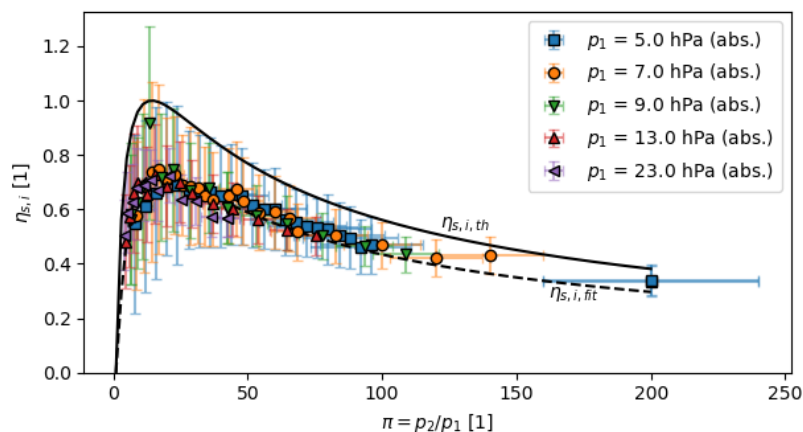

Figure 4: Measured indicated isentropic efficiency $\eta_{s,i}$ for various suction pressures and pressure ratios

The trend of η_i was approximated by Eq. (9), introducing the loss coefficient C_L for inner leakage losses. The loss coefficient $C_L = 0.7817$ was derived from the test data using the least square method.

$$\eta_{s,i,fit} = C_L \eta_{s,i,th}(1 - p_2/p_1) \tag{9}$$

Figure 5 shows the results for the combined mechanical and electrical efficiency $\eta_m \eta_{el}$ over the theoretical indicated power input $P_{i,th}$. The results show that there is a significant dependency of $\eta_m \eta_{el}$ on $P_{i,th}$. For lower $P_{i,th}$, the efficiency decreases, and for higher $P_{i,th}$ the efficiency approaches 0.6. This part load behavior may be attributed to the permanent magnet synchronous motors (PMSM). According to Winzer (2017), PMSM show a decrease in efficiency for low torque operation.
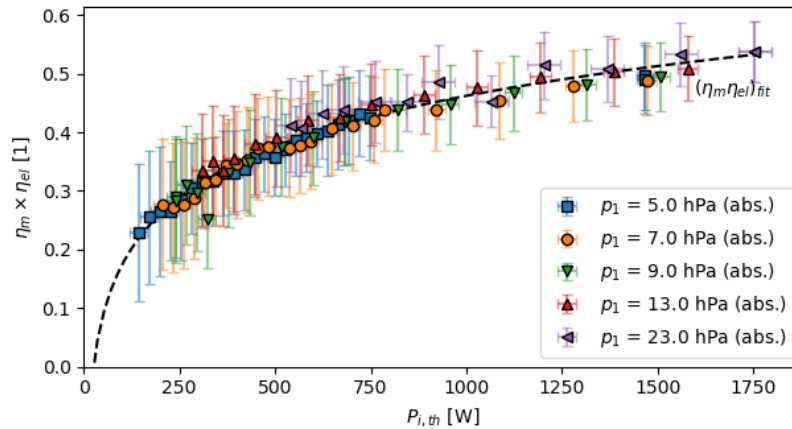
Figure 5: Measured combined mechanical and electrical efficiency $\eta_m \eta_{el}$ over the theoretical indicated power input $P_{i,th}$ for various suction pressures

The trend of $\eta_m \eta_{el}$ was approximated by Eq. (10), introducing the loss coefficients $C_{m,el}$ and $C_{m,el,0}$. The loss coefficients $C_{m,el} = 0.28807582$ and $C_{m,el,0} = -0.40213253$ were derived from the test data using the least square method.

$$(\eta_m \eta_{el})_{fit} = C_{m,el} \cdot \log_{10}(P_{i,th}) + C_{m,el,0} \tag{10}$$

5. POTENTIAL ANALYSIS FOR A R718 CHILLER / HEAT PUMP

The potential of this compressor technology for future R718 chiller or heat pump applications is analyzed with a simple cycle model. The cycle model represents a single stage R718 vapor compression cycle assuming a suction superheat $\Delta T_{SH} = 1.0$ K and a subcooling in the liquid line of $\Delta T_{SC} = 1.0$ K. The evaporation and condensation temperatures were varied between 5 °C $\leq \vartheta_0 \leq$ 20 °C and 30 °C $\leq \vartheta_C \leq$ 100 °C, respectively.

The theoretical maximum cooling capacity is calculated with Eq. (11). For the given evaporation temperatures the maximum cooling capacity ranges from 1.3 kW ($\vartheta_0 = 5$°C) to 3.9 kW ($\vartheta_0 = 20$°C).

$$\dot{Q}_{0,th} = V_{disp} \cdot n \cdot \rho_1 \cdot q_0 \tag{11}$$

with
$$q_0 = h(p_C, T_C - \Delta T_{SC}) - h(p_0, T_0 + \Delta T_{SH});$$
$$\rho_1 = \rho(p_0, T_0 + \Delta T_{SH}); p_0 = p''(T_0); p_C = p''(T_C)$$

The performance of the potential R718 chiller is evaluated with the COP_0 that is defined by Eq. (12). The following analysis focusses on the COP_0. However, the performance for a heat pump may be evaluated by using $COP_H = COP_0 + 1$.

$$COP_0 = q_0 \cdot w_s^{-1} \cdot \eta_{s,i} \cdot \eta_m \eta_{el} \tag{12}$$

$$\text{with} \quad w_s = (h_{2,s} - h_1)$$

Where η_i is calculated with Eq. (9) and $\eta_m \eta_{el}$ is calculated with Eq. (10). For a better comparison with state-of-the-art machines, the performance is also evaluated in regards to the maximum COP_0 assuming a Carnot cycle.

$$COP_{0,Carnot} = T_0 / (T_C - T_0) \tag{13}$$

The potential analysis includes a baseline and an improved case. The baseline case assumes that the tested compressor is directly used for R718. The improved case assumes that the compressor has been modified to reduce the inner leakage and improve the motor, bearings, and inverter. For the improved case the loss coefficient C_L is modified to $C_L^* = C_L + 0.10$ and $C_{m,el,0}$ is modified to $C_{m,el,0}^* = C_{m,el,0} + 0.30$. With these corrections, the inner efficiency $\eta_{s,i}$ reaches an optimal value of 0.88 and the combined mechanical and electrical efficiency $\eta_m \eta_{el}$ approaches 0.9.

Figure 6 shows the results of the performance analysis for both the baseline case (left) and the improved case (right). The results of the baseline case indicate that a R718 chiller/heat pump unit with the current version of the compressor may not be competitive compared to state-of-the-art machines. The maximum COP_0 values are only at approx. 1.5. The results for the improved case show an improvement of the COP_0 to maximum values of around 3.0. The real potential of the R718 chiller/heat pump with spindle screw compressors can be seen for higher temperature lifts ($T_C - T_0$) where the $COP_0/COP_{0,Carnot}$ values are still above 40%. This may enable efficient heat recovery for new chiller units or an extended application range for high-temperature climates. It should be noted, that the compressor performance decreases for small temperature lifts. This is due to the compressor's volume index and the resulting over-compression losses.
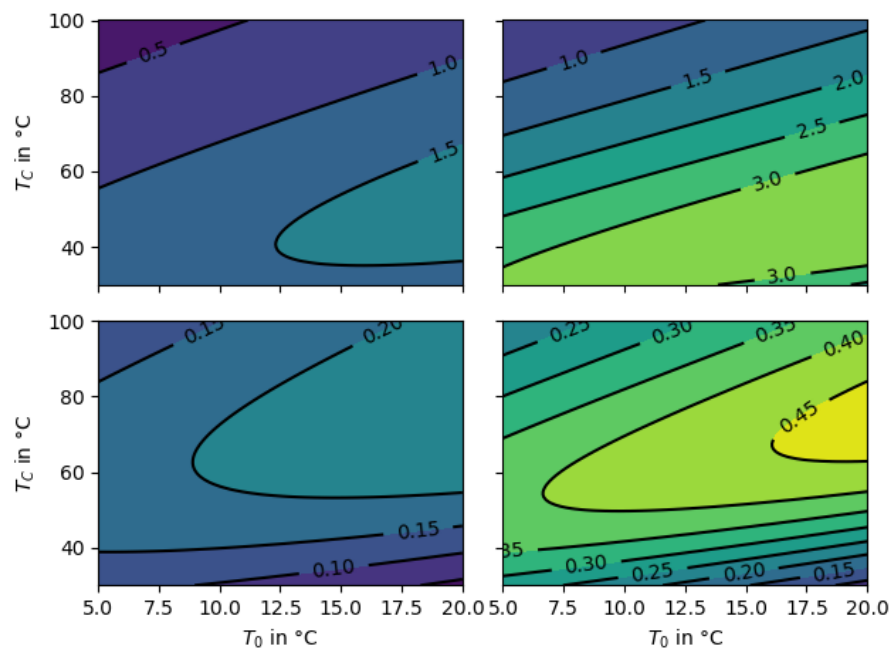
Figure 6: Calculated COP_0 (top) and $COP_0/COP_{0,Carnot}$ (bottom)
for the baseline case (left) and the improved case (right)

6. CONCLUSIONS

This experimental investigation has successfully shown the potential of spindle screw compressors for future R718 chillers and heat pumps with evaporation temperatures of 5°C to 20°C and condensing temperatures of 30°C to 100°C. The volumetric efficiency of the tested compressor ranged from 0.65 to 0.85 and was relatively stable (±0.05) for a wide range of pressure ratios (π = 4 to 200). The indicated isentropic efficiency $\eta_{s,i}$ reached a maximum value of 0.78 which is comparable to other refrigeration compressors, given the wide range of pressure ratios, whereas the combined mechanical and electrical efficiency $\eta_m \eta_{el}$ tended to a maximum of only 0.6. The difference in regards to location of each efficiency's optimum leads to overall isentropic efficiencies of $0.13 \leq \eta_{s,tot} \leq 0.33$. The predicted performance of a potential R718 chiller/heat pump with spindle screw compressors shows that the current design needs to be revised for R718 in terms of profile optimization and powertrain design. The compressors main potential were identified as R718 chillers with an increased temperature lift such as chillers with heat recovery or chillers in high-temperature climates.

NOMENCLATURE

c_m	most probable molecular speed	(m/s)	$\dot{Q}$	heat flow	(W)
c_p	specific heat capacity	(J/kgK)	q	specific heat	(J/kg)
C	loss coefficient	(-)	s	specific entropy	(J/kgK)
COP	coefficient of performance	(-)	T	temperature	(K)
h	specific enthalpy	(J/kg)	ΔT	temperature difference	(K)
h_{min}	min. leakage gap height	(m)	v	specific volume	(m³/kg)
k	Boltzmann constant	(J/K)	V	volume	(m³)
Kn	Knudsen number	(-)	V_i	volume index	(-)
$\dot{m}$	mass flow rate	(kg/s)	$\dot{V}$	volume flow rate	(m³/s)
M	molar mass	(kg/mol)	w	specific work	(J/kg)
n	rotational speed	(1/s)	η	efficiency	(-)
N	Avogadro constant	(1/mol)	ϑ	temperature	(°C)
p	pressure	(Pa)	μ	dynamic viscosity	(Pa s)
$p"$	saturation pressure	(Pa)	π	pressure ratio	(-)
P	power	(W)	ρ	density	(kg/m³)

Subscript

0	evaporation	*i*	indicated / inner	*SC*	subcooling	*v*	volumetric
0…5	state points	*L*	leakage	*SH*	superheat	*w*	cooling water
C	condensing	*m*	mechanical	*suc*	suction		
disp	displacement	*opt*	optimum	*th*	theoretical		
el	electrical	*s*	isentropic	*tot*	overall		

REFERENCES

Bell, I. H., Wronski, J., Quoilin, S., & Lemort, V. (2014). Pure and pseudo-pure fluid thermophysical property evaluation and the open-source thermophysical property library CoolProp. *Industrial & engineering chemistry research*, 53(6), 2498-2508.

Chamoun, M., Rulliere, R., Haberschill, P., & Peureux, J. L. (2014). Experimental and numerical investigations of a new high temperature heat pump for industrial heat recovery using water as refrigerant. *International Journal of Refrigeration*, 44, 177-188.

Coleman, H. W., & Steele, W. G. (2009). *Experimentation, Validation, and Uncertainty Analysis for Engineers*, Jon Wiley & Sons, Inc, New Jersey.

DIN Deutsches Institut für Normung e. V. (1983). *Abnahmeregeln für Rotationsverdrängervakuumpumpen - Sperr- und Drehschieber- sowie Kreiskolbenvakuumpumpen im Grob- und Feinvakuumbereich* (DIN 28426-1).

DIN Deutsches Institut für Normung e. V. (2017). *Kältemittel-Verdichter und Verflüssigungssätze für die Kälteanwendung – Leistungsprüfung und Prüfverfahren – Teil 1: Kältemittel-Verdichter* (DIN 13771-1)

Edler, C., (2013). Entwicklung der Energieeffizienz von Kältemittelverdichtern: *DKV Tagungsbericht 2013 Hannover*, Germany

Hanslik, F., Suess, J., & Koehler, J. (2019). The potential of water as a refrigerant - past, present and future approaches*: Proceedings of the 25th IIR-International Congress of Refrigeration, Montreal, Canada* (2130–2137).

Huck, C., Pleskun, H., & Brümmer, A. (2018). Measurement and simulation of rarefied Couette Poiseuille flow with variable cross section. *Journal of Vacuum Science & Technology A: Vacuum, Surfaces, and Films*, *36*(3), 031606.

Moesch, T. W., Janitschke, T., Thomas, C., & Hesse, U. (2019). Analysis of cycloid type vacuum compressors for water vapor compression systems at sub-atmospheric pressures. In *IOP Conference Series: Materials Science and Engineering* (Vol. 604, No. 1, p. 012008). IOP Publishing.

Winzer, P. (2017). *Steigerung von Drehmoment und Wirkungsgrad bei Synchronmaschinen durch Nutzung der magnetischen Asymmetrie* (Dissertation, Karlsruhe, Karlsruher Institut für Technologie (KIT), 2017).

ACKNOWLEDGEMENT